Model Predictive Control of Regulation Services from Commercial Buildings to the Smart Grid

Mehdi Maasoumy†, Borhan M. Sanandaji*, Alberto Sangiovanni-Vincentelli*, and Kameshwar Poolla*

***Abstract*— We first demonstrate that the demand-side flexibility of the Heating Ventilation and Air Conditioning (HVAC) system of a typical commercial building can be exploited for providing frequency regulation service to the power grid using at-scale experiments. We then show how this flexibility in power consumption of building HVAC system can be leveraged for providing regulation service. To this end, we consider a simplified model of the power grid with uncertain demand and generation. We present a Model Predictive Control (MPC) scheme to direct the ancillary service power flow from buildings to improve upon the classical Automatic Generation Control (AGC) practice. We show how constraints such as slow and fast ramping rates for various ancillary service providers, and short-term load forecast information can be integrated into the proposed MPC framework. Finally, we provide extensive simulation results to illustrate the effectiveness of the proposed methodology for enhancing grid frequency regulation.**

I. Introduction

A sustainable energy future requires widespread and significant penetration of Renewable Energy Sources (RESs). Several states in the U.S. and countries around the world have set ambitious targets for penetration of RESs by the next few years. The state of California, as an example, has targeted a 33% RES portfolio by 2020 [1]. However, volatility, uncertainty, and intermittency of RESs present a challenge for integrating such resources into the power grid in a large scale as proper functioning of the grid requires continuous power balance between supply and demand.

In addition to the need for maintaining balance between generation and load, the power flows through individual transmission lines and facilities should also be continuously controlled by adjusting generation or load. Instantaneous matching between generation and load is even more challenging when considering uncertainties and randomness in demand. Short-term load variability results from a random switching of millions of individual loads. Longer-term variability results from predictable factors such as the daily and seasonal load patterns as well as less predictable events such as shifting weather patterns. Traditional generators may also cause unexpected fluctuations due to a range of equipment failures and aging [2].

Electricity storage is widely believed to be a solution to this problem by absorbing the variability associated with RESs. However, storage has two important drawbacks. It is expensive and it is not environmentally friendly. There is an emerging consensus that flexible loads with thermal storage capabilities such as Thermostatically Controlled Loads (TCLs) will play an important role in regulating the grid frequency and consequently in enabling deep penetration of RESs. It has been reported that about 20% of the total electricity consumption in the United States is used by residential TCLs such as air conditioners, heat pumps, water heaters, and refrigerators [3], [4]. Recently, [5], [6] showed that flexible loads such as TCLs are good candidates for providing ancillary services since their aggregate flexibility has the characteristic of a stochastic battery.

These recent papers also demonstrate that TCLs have a great potential for providing *fast* regulating reserve services; speed is indeed beneficial, especially in the context of recent regulations such as Federal Energy Regulatory Commission (FERC) Order 755 [7]. In fact, these new federal regulations require scheduling coordinators to procure and compensate more for regulation resources with *faster ramping rates*. There is an emerging consensus that future regulation services will be distinguished and compensated by *capabilities* of which ramping rate is one component.

Modeling, estimation, and control of aggregated heterogeneous TCLs for ancillary services have been discussed in [8], [9]. TCLs are particularly well-suited for Direct Load Control (DLC) and Demand Response (DR) programs that require loads to both decrease and increase power consumption because they are capable of storing thermal energy, much like a battery stores chemical energy. Fully responsive load control is highlighted in [10] in the context of TCLs and plug-in Electric Vehicles (EVs). Despite several challenges of using loads for system services, several key advantages include: 1) Reducing overall grid emissions by using loads to provide system services [11]. 2) Instantaneous response of loads to operator requests, versus slow response of generators to make significant output changes [12], and 3) Less variability associated to a very large number of small loads with respect to that of a small number of large generators [12]. It may soon be the case that the only technical impediment to reliable utilization of loads for system services is the development of the necessary load models and control strategies and the development of inexpensive and scalable communication and sensing infrastructure. [13].

In this paper, we first quantify (by means of empirical data analysis) the demand-side flexibility of a typical commercial building. Then we show that such flexibility can be tapped for providing fast frequency regulation service to the power grid. We then show the effectiveness of such "fast" ramping rates on the overall frequency regulation performance in the event of transient fluctuations in the load. To this end, we consider a simplified model of the power grid with uncertain demand and generation. We present a Model Predictive Control (MPC) scheme to control the ancillary

† Department of Mechanical Engineering, University of California, Berkeley, CA 94720, USA. Corresponding author. Email: mehdi@me.berkeley.edu

* Department of Electrical Engineering and Computer Sciences, University of California, Berkeley, CA 94720, USA.

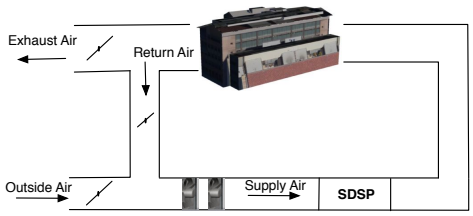

Fig. 1. Schematics of the experiment testbed (Sutardja-Dai Hall on UC Berkeley campus).

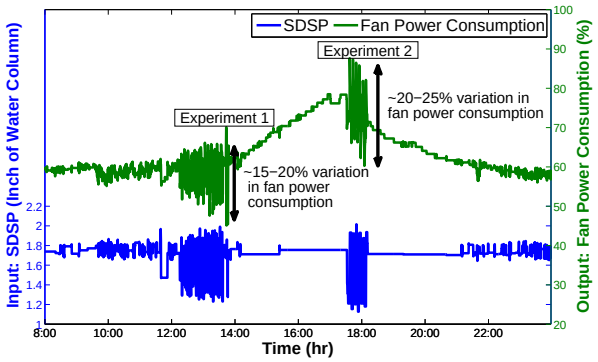

Fig. 2. Fan power consumption can vary as quickly as in a few seconds by up to 25% by changing the SDSP set-point.

service power flow from buildings to improve on the classical Automatic Generation Control (AGC) practice, by integrating information such as ramping rates of various sources of regulation services, and short term load forecast into the control algorithm. We provide extensive simulation results to illustrate the effectiveness of the proposed methodology for enhancing grid frequency regulation.

The paper is organized as follows. A high-level description of the test bed, a summary and the results of the experiments performed on the test bed is provided in Section II which quantifies the amount of flexibility of the building power consumption. The mathematical model describing the dynamics of the power system is followed in Section III. AGC is explained in Section IV. Our proposed MPC scheme is explained in details in Section V. We provide extensive simulation results in Section VI. Future work and conclusion remarks are provided in Section VII.

II. Fast Ancillary Power from Buildings

Commercial buildings consume more than 35% percent of electricity in the US [14]. About 15% of electricity consumption in commercial buildings is related to the fans of the heating, ventilation and air conditioning (HVAC) systems. HVAC fans are essential parts of HVAC systems in buildings that move the conditioned air from the air handling units (AHU) to the room level for ventilation, heating and cooling of building indoor climate [15]–[17]. For instance, the main supply fans that feed Sutardja-Dai Hall (SDH) on the UC Berkeley campus can spin at variable speeds. Power consumption is proportional to the cube of fan speed, with

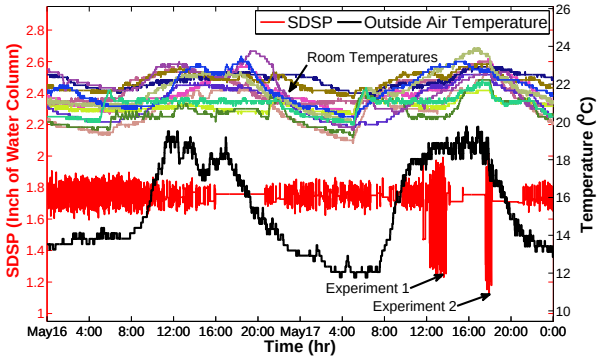

Fig. 3. SDSP set-point, outside air temperature, and temperature of 15 randomly selected rooms are shown for one day before (May 16, 2013) and the day of the experiment (May 17, 2013).

the maximum rated power of 134 KW or about 14% of the maximum power consumed in that building. Moreover, more than 30% of commercial buildings have adopted Building Energy Management System (BEMS) technology, which facilitates a fine control of the building HVAC components as well as the communication with the grid system operators. The majority of commercial buildings are also equipped with variable frequency drives, which in coordination with BEMS, can manipulate the HVAC system power consumption very frequently (in the order of seconds).

The supply fans to the building consume a large amount of power and have inherent flexibility in how they consume electricity. Hence, as shown in [18] we can directly modulate HVAC power consumption, within a safe envelope, without imposing extra cost to the building operation, and violating occupant comfort constraints. This flexibility in power consumption can be either upward (consuming more) or downward (consuming less), making it an ideal candidate for regulation services.

A. Experiment Results

To demonstrate this potential of commercial building HVAC system, we performed at-scale experiments on the HVAC system of Sutardja-Dai Hall on the UC Berkeley campus. The goal of the experiment was to quantify this flexibility, and to examine the effects of supply-fan speed modulation on the internal temperature of the rooms in the building. More details on the experiments is reported in [19]. Here we present a summary and the results of the experiments to set a foundation for the rest of the paper.

Fig. 1 shows a high-level schematics of our experiment set-up including the main fans that feed Sutardja-Dai Hall. The speed of the fans is indirectly controlled by setting the Supply-Duct Static Pressure (SDSP) set-point value. The main challenges in performing this experiment include 1) keeping the pressure in the air ducts within a specific safety boundary and 2) minimizing the changes on the internal temperature that may make occupants uncomfortable. Because of the first concern, we used the SDSP set-point to control fan speed, instead of directly changing the fan

speed by over-writing its control logic. The safety margin for the pressure set-point ranges between $[1.2 - 1.9]$ (Inch of Water Column). By changing the SDSP set-point, the fan speed either increased or decreased to adhere to the specified pressure value. We also tested the response speed of the fans to respond to changes to the pressure set-point and model the response. We run a number of experiments where we vary the speed of the fan at different rates and for different lengths of time. We show that supply-fan speed modulation, over short time periods, has little effect on the comfort of the building occupants. In fact, the effects are not observable on the internal temperature of the spaces. We also show that the supply fan responds very quickly to a change in the pressure set-point, indicating that this is a viable option for providing grid-level ancillary response services.

The experiment results are shown in Fig. 2 and Fig. 3. Fig. 2 shows the SDSP set-point signal, as the input of the experiment and the power consumption of the fan, as the output of the experiment. It is observed that the fan power consumption can vary by up to 25% within a few seconds around its nominal power consumption at each time (which itself is prescribed by the control logic running the HVAC system). Fig. 3 on the other hand shows the SDSP set-point, the outside air temperature and temperature of 15 randomly selected rooms in the building. This figure is provided to show that the performed experiment created no significant and human-sensible change in the temperature of the building, and the building temperature was kept within the comfort zone at all times. Data of one day before the experiment (May 16) and the day of experiment (May 17) is provided for comparison. Based on the experiment results it was estimated in [19] that in average, each fan can provide about 18% of its nominal power as flexibility. This equals 12 kW out of 67 kW power draw for each fan, and in total 24 kW for the whole SDH building.

B. Total Ancillary Power From All US Commercial Buildings

According to the latest survey on energy consumption of commercial buildings, performed in 2003 [14], there are 4.9 million commercial buildings in the US which cover a total area of about 72 billion square feet. Almost 30% of these buildings are equipped with variable frequency drive fans. Assuming the same fan power consumption flexibility per square foot for these buildings to that of SDH, we estimate that at least 4 GW of fast ancillary service is readily available in the US at almost no cost, based on the 2003 data. Commercial building floor space is expected to reach 103 billion sq. ft. in 2035 [20]. With the same assumption of the above calculations, about 5.6 GW of regulation reserve will be available in 2035.

We also identify a Single-Input Single-Output (SISO) Auto Regressive with eXogenous input (ARX) model of the fan with SDSP as input and fan power consumption as output based on the empirical data from SDH building. In order to track the SDSP signal, the two fans change their speeds and consequently their power consumption changes. A detailed description of the experiments and analysis on the results has been reported in [19].

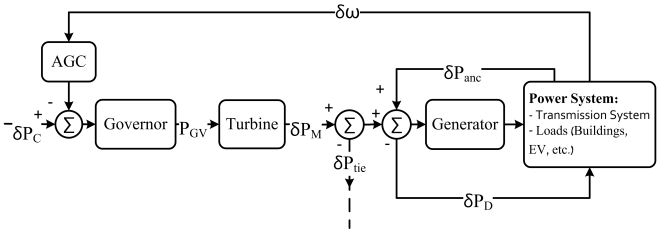

Fig. 4. Block diagram of power system and its relation to governor, turbine, generator, and the AGC signal for each control area.

III. Mathematical Models of Power System Components

In this section, we develop mathematical models of power system components. These models, along with the estimations on the amount of available ancillary power from buildings, obtained from the experiment results of Section II, and the proposed control algorithm of Section V, will be used to demonstrate how commercial buildings flexibility can be utilized for frequency regulation provision in the smart grid.

Detailed models of power system elements have been developed in the literature. In this paper, we use the model developed by [21]–[23]. We present a detailed governor, turbine, and generator model in this section. The interconnection of these components of the power system is shown in the block diagram of Fig. 4. δP_C is a control input which acts against increase or decrease in the power demand to regulate the system frequency. δP_D denotes the fluctuations in the power demand which is considered here as an exogenous input (disturbance). We present a model of the power system, with the following underlying assumptions:

- The resistance of the transmission lines are ignored.
- Transmission line between area i, and j is characterized by a reactance $X_{\text{tie}_{ij}}$.
- Reactive power flows are ignored.
- Voltage of bus i, denoted by V_i is considered constant.

Under steady state, we have: $\omega = \omega_o$, $V_t = V_t^o$, and $P_M = P_G = P_M^o$, where ω_o, V_t^o, and P_M^o are the nominal values for rated frequency, terminal voltage and mechanical power input. Basic variables of a power system which are used in the following formulations with a short description of each variable are reported in Table I.

A. Governor Model

A general model of a governor contains three time constants. The overall input-output transfer function is given by

$$T_{Gov}(s) = \frac{(1 + sT_2)}{(1 + sT_1)(1 + sT_3)}. \tag{1}$$

Mechanical-hydraulic governors have $T_2 = 0$ with typical values of $T_1 \in [0.2, 0.3]$ and $T_3 = 0.1$. Electro-hydraulic governors without steam feedback have typical time constants as follows: $T_1 = T_2 = 0$ and $T_3 \in [0.025, 0.1]$. Electro-hydraulic governors with steam feedback utilize a

TABLE I

BASIC POWER SYSTEMS NOMENCLATURE

Variables	Description
P_M	Mechanical power input
P_M^o	Desired real power generation
P_G	Generated real electric power
δP_G	Increase in demand (at rated generator MVA)
V_t	Terminal voltage
P_D	Load (Power Demand)
δP_D	Input disturbance due to load changes
δP_C	Speed changer position feedback control signal
ω	Angular speed and frequency
ω_o	Rated (desired) frequency
Parameters	**Description**
D	Damping coefficient. Range: 0.01 - 0.1 [-]
M	Machine inertia constant. Range: 100 - 1000 [MW s]
R	Speed regulation constant. Range: 0.05 [p.u.]
T_i	Time constant for power system components. Range: {0,0.01-10} [s]
K_i	Fraction of total mechanical power outputs associated with different operating points of the turbine. Range: {0,0.1-1} [-]

feed-forward mechanism. Typical time constant values under these assumptions are as follows: $T_1 = 2.8$, $T_2 = 1.0$, and $T_3 = 0.15$ [21].

B. Turbine Model

Turbines are grouped into steam and hydro turbines. The input-output transfer function model for turbines is given by

$$\frac{\delta P_M}{P_{GV}} = K_1F_1 + K_3F_1F_2 + K_5F_1F_2F_3 + K_7F_1F_2F_3F_4, \quad (2)$$

where F_1, F_2, F_3, and F_4 are transfer functions corresponding to steam chest, piping system, re-heaters, and cross-over mechanisms, respectively, and are given by

$$F_1(s) = \frac{1}{1+sT_4}, \qquad F_2(s) = \frac{1}{1+sT_5}, \quad (3)$$

$$F_3(s) = \frac{1}{1+sT_6}, \qquad F_4(s) = \frac{1}{1+sT_7}. \quad (4)$$

The basic time constant associated with steam turbines is T_4 which corresponds to that of the *steam chest*. For non-reheat steam turbines, this is the only time constant needed. The time constants T_5, T_6, and T_7, are associated with time delays of piping systems for re-heaters and cross-over mechanisms. The coefficients K_1, K_3, K_5, and K_7 represent fractions of total mechanical power outputs associated with *very high*, *high*, *intermediate*, and *low* pressure components, respectively. Typical values of steam turbine time constants and fractions are reported in [21].

C. Generator Model

The dynamics of the generator is given by the following transfer function

$$F_{Gen} = \frac{1}{D+sM}, \quad (5)$$

where constants D and M represent the damping coefficient and the inertia of the governor, respectively.

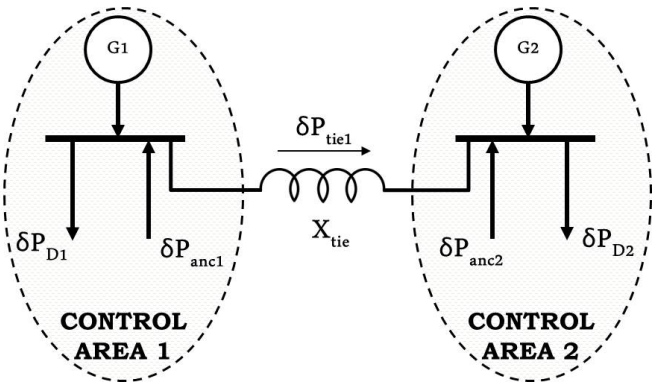

Fig. 5. Two control area system. Each control area includes a generation unit. δP_{D_i} and $\delta P_{\mathrm{anc}_i}$ are load (demand) and ancillary power in area i.

D. Two Area System Model

Consider the interconnected system shown in Fig. 5. It consists of two areas connected by a tie line with reactance X_{tie}. The power flow on the tie line from area 1 to area 2 is shown by P_{tie}. A positive δP_{tie} represents an increase in power transfer from area 1 to area 2. This in effect is equivalent to increasing the load of area 1 and decreasing the load of area 2. Each area consists of the subsystems shown in Fig. 4.

Next, we present the mathematical model of the entire system. Note that the superscript refers to the control area (i or $j = 1, 2$ in the case of two interconnected areas), and the subscript indexes the state in each area.

$$\frac{dx_1^i}{dt} = \frac{(-D^i x_1^i + \delta P_M^i - \delta P_D^i - \delta P_{\mathrm{tie}}^{ij} + \delta P_{\mathrm{anc}}^i)}{M_x^i} \quad (6a)$$

$$\frac{dx_2^i}{dt} = \frac{(x_3^i - x_2^i)}{T_7^i} \quad (6b)$$

$$\frac{dx_3^i}{dt} = \frac{(x_4^i - x_3^i)}{T_6^i} \quad (6c)$$

$$\frac{dx_4^i}{dt} = \frac{(x_5^i - x_4^i)}{T_5^i} \quad (6d)$$

$$\frac{dx_5^i}{dt} = \frac{(P_{GV}^i - x_5^i)}{T_4^i} \quad (6e)$$

$$\frac{dx_6^i}{dt} = \frac{(x_7^i - x_6^i)}{T_3^i} \quad (6f)$$

$$\frac{dx_7^i}{dt} = \frac{(-x_7^i + \delta P_C^i - x_1^i/R^i)}{T_1^i} \quad (6g)$$

where

$$\delta P_M^i = K_1^i x_5^i + K_3^i x_4^i + K_5^i x_3^i + K_7^i x_2^i \quad (7)$$

$$P_{GV}^i = (1 - T_2/T_3)x_6^i + (T_2/T_3)x_7^i \quad (8)$$

In formulation (6), the first state represents the frequency increment, $x_1^i = \delta\omega_i$. All the seven states are derived using the mathematical model of each subsystem as presented in (1)–(5). Note that when the time constant representing the system pole is zero, the corresponding differential equation becomes an algebraic equation. For instance, when $T_5 = 0$, the equation $\frac{dx_4^i}{dt} = 1/T_5(x_5^i - x_4^i)$ becomes $x_5^i = x_4^i = 0$.

The real transferred power from bus i to bus j is governed by $P_{\text{tie}}^{ij} \approx V_i V_j b_{ij} cos(\theta_i - \theta_j)$. Since here we are concerned with incremental changes in all variables, the incremental change in P_{tie}^{ij} is given by $\delta P_{\text{tie}}^{ij} = \nu_{ij}(\theta_i - \theta_j)$ where at the nominal operating points, θ_i^o, $i = 1, 2$, the *transmission line stiffness* coefficient ν_{ij} is given by

$$\nu_{ij} = -V_i V_j b_{ij} cos(\theta_i^o - \theta_j^o). \tag{9}$$

In terms of the incremental state variables used, we have:

$$\delta P_{\text{tie}}^i = \sum_{j=1}^{n} \nu_{ij}(x_8^i - x_8^j), \tag{10}$$

where the state variable x_8^i is the integral of the frequency increment of area i, i.e.,

$$\frac{dx_8^i}{dt} = x_1^i. \tag{11}$$

The state space model (6)-(11) can be written in compact form as follows:

$$\frac{dx(t)}{dt} = A'x(t) + B_1' u_{sc}(t) + B_2' u_{anc}(t) + E'd(t). \tag{12}$$

In the case of two areas, states are stored in x, input signals to the speed changers are $u_{\text{sc}} = [\delta P_{C_1}\ \delta P_{C_2}]^T$, the ancillary inputs buildings are $u_{\text{anc}} = [\delta P_{\text{anc}_1}\ \delta P_{\text{anc}_2}]^T$, and the exogenous input (disturbance) (*i.e.* variations in demands) are denoted by $d = [\delta P_{D_1}\ \delta P_{D_2}]^T$.

E. Load Modeling

Many loads are frequency-sensitive. In this case, the incremental change in load will have a frequency-dependent part, i.e.

$$\delta P_D = \delta P_D^o + \bar{D}\delta\omega \tag{13}$$

where $\bar{D} = \frac{\partial P_D}{\partial \omega}$ represents the sensitivity of the load to frequency changes at the nominal value of the load. In this case, D^i in (6a) is replaced by $D^i + \bar{D}^i$, and δP_D is replaced by δP_D^o.

F. Discretization of the Continuous Model

We discretize the state space dynamics of the system using the forward Euler discretization scheme. We show the result of the equation for $\dot{x}_1^i$. The discretized dynamics for the rest of the states can be obtained in similar way. At time t_n we approximate the derivative of x_1^i by

$$\frac{dx_1^i(t_n)}{dt} \approx \frac{x_1^i(t_n + \delta t) - x_1^i(t_n)}{\delta t} \tag{14}$$

Hence the discretized version of (6a) is

$$x_1^i(t_{n+1}) = (1 - \frac{D_x^i \delta t}{M_x^i})x_1^i + \frac{\delta t}{M_x^i}\left[\delta P_M^i - \delta P_D^i - \delta P_{\text{tie}}^{ij} + \delta P_{\text{anc}}^i\right],$$

where $t_{n+1} = t_n + \delta t$ and δt is the discretization time step. The discrete-time state-space model is obtained as

$$x[k+1] = Ax[k] + B_1 u_{\text{sc}}[k] + B_2 u_{\text{anc}}[k] + Ed[k]. \tag{15}$$

We use this state update equation in Section V where we present the MPC formulation.

IV. Automatic Generation Control

AGC is the main control function of a utility's energy control section. The purpose of an AGC is to track the load variations while maintaining the system frequency, net tie-line interchanges, and optimal generation level close to scheduled values [21]. This function is referred to as Load-Frequency Control (LFC). A secondary objective is to distribute the required change in generation among units to minimize operating cost [23]. In the case where several utilities are interconnected, each will perform its own AGC independent of the others.

With primary speed control action, a change in the system load will result in a steady-state frequency deviation, depending on the governor droop characteristics and frequency sensitivity to the load. All generating units on speed control will contribute to the overall change in generation, irrespective of the location of the load change. Restoration of system frequency to nominal value requires supplementary control action which adjusts the load reference set-point (through the speed-changer motor). Therefore, the basic means of controlling prime-mover power to match variations of system load in a desired manner is through control of the load reference set-points of selected generating units. As system load is continually changing, it is necessary to change the output of generators automatically.

A. AGC in Interconnected Power Systems

In the classical AGC, a simple PI control is utilized to regulate the frequency of the grid. The Area Control Error (ACE) is defined to be

$$ACE^i = \delta P_{tie}^i + \beta^i x_1^i, \tag{16}$$

where $\delta P_{\text{tie}}^i = P_{\text{tie}}^i - P_{\text{tie,scheduled}}^i$, and β^i is the bias coefficient of area i. The standard industry practice is to set the bias β^i at the so-called Area Frequency Response Characteristic (AFRC) which is defined as $\beta^i = D^i + 1/R^i$. The integral of the ACE is then used to construct the speed changer position (δP_C^i) feedback control signal. A new state x_9^i, is defined as

$$\frac{dx_9^i}{dt} = ACE^i. \tag{17}$$

Consequently the control input δP_C^i is given by

$$\delta P_C^i = -K^i x_9^i, \tag{18}$$

where K^i is the feedback gain. We propose a methodology for the ancillary services from buildings to help with the primary control of AGC as describe in V.

V. Model Predictive Control of Ancillary Services

We present an MPC scheme to control the available ancillary service from commercial buildings to improve on the classical AGC practice. This optimization-based control framework is utilized as a *higher-level* control in a "hierarchical" fashion on top of the *low-level* classical AGC control. Consider the n-control area network shown in Fig. 6.

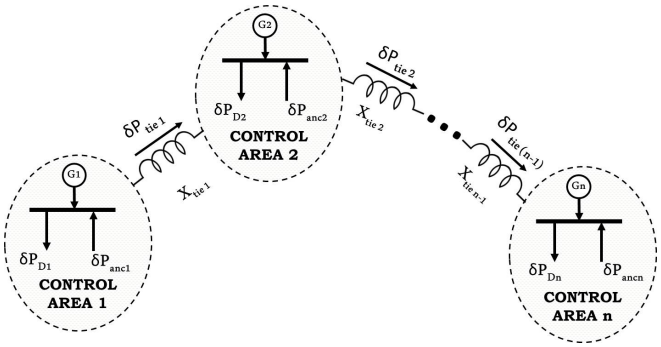

Fig. 6. Schematic of n control areas with their corresponding tie power transfers and reactances.

A. Control Architecture

The schematic of the power system is depicted in Fig. 7. Electric power is generated by the turbo-generators, and is fed to the power system. The power system transmits and distributes the power to the end use.

As mentioned earlier, the recent FERC Order 755 requires scheduling coordinators to procure and compensate more for regulation resources with *faster ramping rates*. To this end, we particularly address such constraints in our proposed MPC framework. In total, we consider the ramping rate constraint, $|P_{\text{anc}}[k+1]-P_{\text{anc}}[k]|$, the maximum capacity, $\max(P_{\text{anc}}[k]) > 0$, and the minimum capacity, $\min(P_{\text{anc}}[k]) < 0$, on the characteristics of the ancillary service signal from commercial buildings. We should mention that buildings can provide both positive and negative power flow to the grid, for frequency regulation purposes. When there is a power deficit, buildings will temporarily use less power, and when there is as surplus of power, they will temporarily use the extra power. We assume that the rate of power supply by the buildings is limited by

$$|\Delta P_{\text{anc}}| \leq \lambda, \tag{19}$$

where

$$\Delta P_{\text{anc}} := P_{\text{anc}}[k+1] - P_{\text{anc}}[k].$$

B. MPC Algorithm

At each time step k, we solve the following optimization problem:

$$\min_{U_{\text{anc}}[k]} \quad \sum_{i=1}^{n}\sum_{j=0}^{H-1}(\text{ACE}^i[k+j|k])^2 \tag{20}$$

$$\text{s.t.} \quad x[k+j+1|k] = Ax[k+j|k] + B_2 u_{\text{anc}}[k+j|k] + Ed[k+j|k]$$
$$\underline{\pi}[k+j|k] \leq u_{\text{anc}}[k+j|k] \leq \overline{\pi}[k+j|k]$$
$$|u_{\text{anc}}[k+j+1|k] - u_{\text{anc}}[k+j|k]| \leq \lambda[k+j|k]$$

where

$$U_{\text{anc}}[k] = (u_{\text{anc}}[k|k], u_{\text{anc}}[k+1|k], \ \ldots, u_{\text{anc}}[k+H-1|k])$$

is the vector of inputs from k to $k+H$, n is the number of areas that participate in this regulation program, and

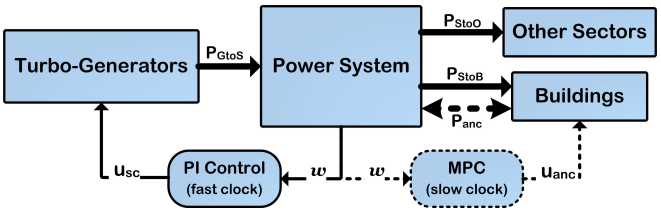

Fig. 7. Schematic of power system and its relation to turbo-generator and and other sectors including the building sector, along with the control architecture. The thick arrows represent the flow of power and the thin arrows represent frequency and control signals. The dashed arrows indicate the additional signals and power flows proposed in this paper.

TABLE II
PARAMETERS FOR THE TWO AREAS USED IN THE SIMULATIONS

Control Area	Parameters
Area 1	$T_1 = 0.1$, $T_3 = 0.1$, $T_4 = 1.0$
	$K_1 = 1.0$
	$M = 132.6$ $(MW.sec)$
	$D = 0.0265$ $(p.u.)$
Area 2	$T_1 = 0.2$, $T_3 = 0.3$, $T_4 = 0.1$, $T_5 = 0.5$
	$K_1 = 0.2$, $K_3 = 3$
	$M = 663.13$ $(MW.sec)$
	$D = 0.1325$ $(p.u.)$

H is the prediction horizon of MPC. Notation $x[k+j|k]$ means that at each time step k, predictions of x for future times $k+j$ are obtained at time k. All the constraints of problem (20) should hold for $j = 0, 1, \ldots, H-1$. The cost function of this optimization problem minimizes the ℓ_2 norm of the ACE signal in areas $i = 1, 2, ..., n$, by exploiting the ancillary service available form buildings, taking into account the system dynamics and constraints. The constraints of the optimization problem are $\overline{\pi}[k+j|k] > 0$ maximum positive power and $\underline{\pi}[k+j|k] < 0$ maximum negative power provided by the participating set of buildings in each area in the contract. Here, "positive" and "negative" refer to the flow of power from generation to consumption. These values are estimated on the building side and sent to the utility periodically. $\lambda[k+j|k]$ is the maximum limit on the rate of change of ancillary service provided by the building side. Note that in the state-space model used in the MPC problem, we do not incorporate $B_1 u_{sc}[k]$ as u_{sc} is assumed to be constant and is regulated by the local PI controller. Fig. 7 illustrates the structure of our MPC implementation with regards to other components of the power system.

VI. SIMULATION RESULTS

We consider two interconnected control areas with parameters of their models presented in Table II, and with inter-area stiffness coefficient of $\nu = 1.0$ $(p.u.)$. The main generation unit for area 1 is a non-reheat turbo generator (TG) system and the main generation unit for area 2 is a hydro TG system. Some metrics such as root mean square (rms) values of frequency and ACE signal are considered to compare the performances of the proposed controller. We use time-invariant bounds on the maximum and minimum ancillary power $\overline{\pi}[k] = \underline{\pi}[k] = \pi$, and maximum rate of change of ancillary power $\lambda[k] = \lambda$, in the following simulations.

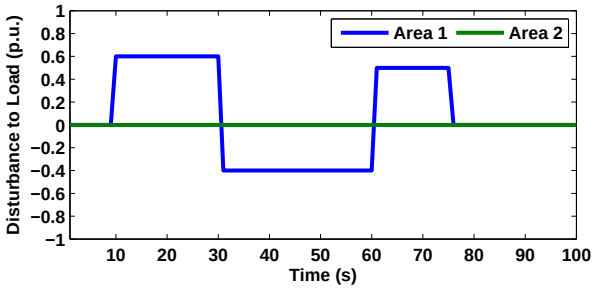

Fig. 8. Disturbance to load in area 1.

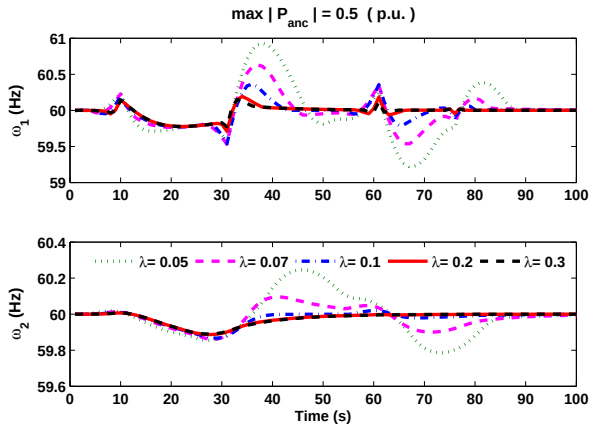

Fig. 9. Frequency of areas 1 and 2 in response to the disturbance are shown. Prediction horizon is $H = 10$ and maximum ancillary power is $\max(P_{\text{anc}}) = 0.5$ $(p.u.)$. Results are for various values of rate of change of ancillary power such that $\max|\Delta P_{\text{anc}}| = \lambda$.

The resulting quadratic program (QP) obtained in Section V-B was formulated using YALMIP [24] and solved with ILOG CPLEX Barrier Optimizer [25] for a time horizon of 100 s and a sampling time $T_s = 1$ s. On a 4-core 2.67-GHz Intel processor with 3.86 GB of memory, the average and maximum solver times were 0.02 s and 0.03 s, respectively, for a prediction horizon of $H = 10$.

We consider a disturbance in the load of area 1, and no disturbance in the load of area 2, as shown in Fig. 8. We assess the performance of the proposed controller considering the following scenarios:

Scenario 1: The maximum ancillary service available in each area is 0.5 per unit (p.u.) of power. We consider a prediction horizon of H=10 time steps. As shown in Fig. 9 by increasing the maximum rate of change of ancillary power (also known as ramping rate for generation units) the resulting frequency deviation decreases. Ramping rate of $\lambda = 0.05$ (p.u./s) is associated with large power generator size, ramping rate of $\lambda = 0.1$ (p.u./s) is associated with smaller size generators and high ramping rates such as $\lambda = 0.3$ (p.u./s) is associated with fast ancillary service such as the one provided by building HVAC system fan.

Scenario 2: We consider a fixed ancillary ramping rate of $\lambda = 0.9$ (p.u./s), and show the frequency deviations in cases with different maximum available ancillary power in each area. The ramping rate is considered very high to eliminate the effects of slow ramping rates on the results, so that we can perform a fair comparison which only concerns the effect of maximum ancillary power. As shown in Fig. 10 by increasing the maximum available ancillary power, the frequency deviation decreases. Although the disturbance in load of area 1 affects both interconnected areas, the change of frequency in area 1 is larger than that of area 2.

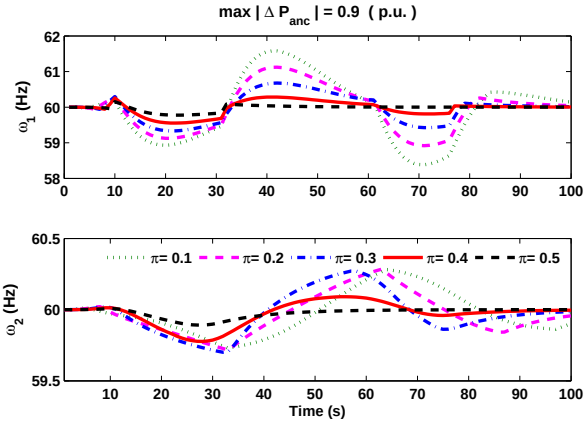

Fig. 10. Prediction horizon is $H = 10$ and the maximum ancillary power is $\max(\Delta P_{\text{ancs}}) = 0.9$ $(p.u.)$. Figure shows frequency of control areas 1 and 2. In each case, we change $\max|P_{\text{anc}}| = \pi$.

Scenario 3: We consider a stronger disturbance and compare the overall frequency and area control error in rms sense. We consider a zero mean disturbance to both areas with a maximum absolute value of ancillary power of $\pi = 0.4$ (p.u.) as shown in Fig. 11. We then perform a mass simulation using various maximum ancillary power available in each area within the range $[0.1\ 0.9]$ (p.u.), and various rate of change of ancillary service within the range $[0.05\ 0.9]$ (p.u./s), and prediction horizons ranging from 1 to 20 time steps.

As shown in Fig. 12, the highest and lowest ACE_{rms} are obtained for the set $\{\pi = 0.1,\ \lambda = 0.02\}$, and the set $\{\pi = 0.9,\ \lambda = 0.9\}$, respectively.

Finally we present the results on the effect of integrating load forecast in the MPC framework. We consider a constant maximum available ancillary power of $\pi = 0.9$ (p.u.) and present the results of rms of frequency deviation for various values of rate of change of ancillary power λ versus prediction horizon as shown in Fig. 13. Short term load forecast can be very valuable and can dramatically improve the performance of the controller. for prediction values up to about $H = 10$, the performance keeps improving, while for longer load forecasts, the improvement is not as significant.

VII. Conclusion and Future Work

We proposed an MPC framework acting in collaboration with a conventional AGC. The proposed MPC integrates information such as different ramping rates of various providers of regulation services, and load forecast to improve the overall system performance. Based on simulation results, we showed how the proposed MPC-based control

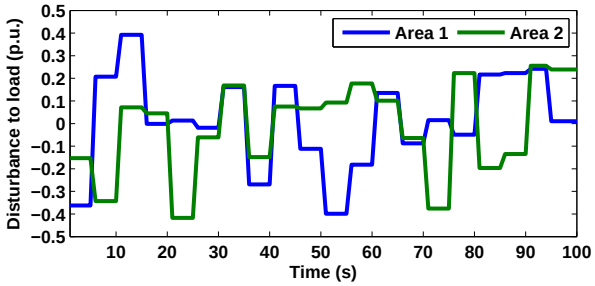

Fig. 11. Disturbance in load of area 1 and 2 used for the mass simulations.

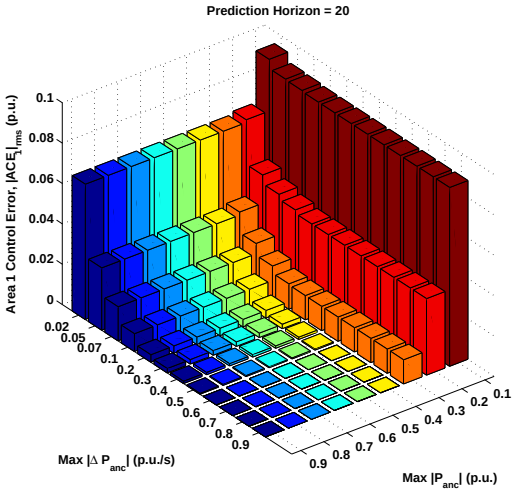

Fig. 12. Result of mass simulation for various maximum ancillary power and maximum rate of change of ancillary power for Prediction horizon of 20 time steps.

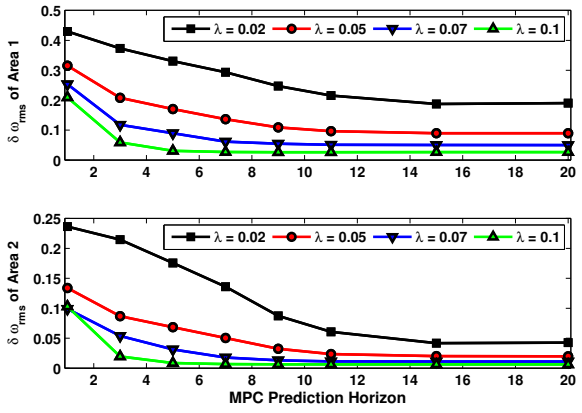

Fig. 13. Root mean square of frequency deviation for various λ values for a constant $\pi = 0.9$ versus prediction horizon.

scheme manages regulation services offered by commercial buildings.

Since it is very difficult to accurately forecast power consumption, as future work, we plan to develop a robust MPC framework to address the uncertainties associated with imperfect predictions of load.

REFERENCES

[1] U. Helman, "Resource and transmission planning to achieve a 33% RPS in California–ISO modeling tools and planning framework," in *FERC Technical Conference on Planning Models and Software*, 2010.

[2] B. Kirby, *Frequency regulation basics and trends*. United States. Department of Energy, 2005.

[3] "Buildings energy data book." [Online]. Available: http://buildingsdatabook.eren.doe.gov/default.aspx

[4] "U.S. Energy Information Administration, annual energy review," 2010. [Online]. Available: http://www.eia.gov/totalenergy/data/annual/#consumption

[5] B. M. Sanandaji, H. Hao, and K. Poolla, "Fast regulation service provision via aggregation of thermostatically controlled loads," *to appear in Proceedings of 47-th Hawaii International Conference on System Sciences – HICSS47*, 2014.

[6] H. Hao, B. M. Sanandaji, K. Poolla, and T. L. Vincent, "Aggregate flexibility of thermostatically controlled loads," *submitted to the IEEE Transactions of Power Systems*, 2013.

[7] "Frequency energy regulation compensation - FERC order no. 755," MISO, Tech. Rep., March 2013. [Online]. Available: https://www.midwestiso.org

[8] S. Koch, J. Mathieu, and D. Callaway, "Modeling and control of aggregated heterogeneous thermostatically controlled loads for ancillary services," in *Proc. PSCC*, 2011, pp. 1–7.

[9] J. Mathieu and D. Callaway, "State estimation and control of heterogeneous thermostatically controlled loads for load following," in *System Science (HICSS), 2012 45th Hawaii International Conference on*. IEEE, 2012, pp. 2002–2011.

[10] D. Callaway and I. Hiskens, "Achieving controllability of electric loads," *Proceedings of the IEEE*, vol. 99, no. 1, pp. 184–199, 2011.

[11] G. Strbac, "Demand side management: Benefits and challenges," *Energy Policy*, vol. 36, no. 12, pp. 4419–4426, 2008.

[12] B. Kirby, *Spinning reserve from responsive loads*. United States. Department of Energy, 2003.

[13] C. Woo, E. Kollman, R. Orans, S. Price, and B. Horii, "Now that california has ami, what can the state do with it?" *Energy Policy*, vol. 36, no. 4, pp. 1366–1374, 2008.

[14] Commercial Buildings Energy Consumption survey (CBECS) . [Online]. Available: http://www.eia.gov/consumption/commercial/data/2003/index.cfm?view=consumption

[15] M. Maasoumy, "Modeling and optimal control algorithm design for HVAC systems in energy efficient buildings," Master's thesis, EECS Department, University of California, Berkeley, Feb 2011. [Online]. Available: http://www.eecs.berkeley.edu/Pubs/TechRpts/2011/EECS-2011-12.html

[16] F. Oldewurtel, A. Parisio, C. Jones, M. Morari, D. Gyalistras, M. Gwerder, V. Stauch, B. Lehmann, and K. Wirth, "Energy efficient building climate control using stochastic model predictive control and weather predictions," in *American Control Conference (ACC), 2010*. IEEE, 2010, pp. 5100–5105.

[17] Y. Ma, F. Borrelli, B. Hencey, B. Coffey, S. Bengea, and P. Haves, "Model predictive control for the operation of building cooling systems," in *American Control Conference (ACC), 2010*. IEEE, 2010, pp. 5106–5111.

[18] M. Maasoumy, C. Rosenberg, A. Sangiovanni-Vincentelli, and D. Callaway, "Model predictive control approach to online computation of demand-side flexibility of commercial buildings hvac systems for supply following," in *submitted to the American Control Conference (ACC)*, 2014.

[19] M. Maasoumy, J. Ortiz, D. Culler, and A. Sangiovanni-Vincentelli, "Flexibility of commercial building hvac fan as ancillary service for smart grid," in *submitted to the IEEE Green Energy and Systems Conference (IGESC)*, 2013.

[20] EIA (2012) Annual energy Outlook 2012. . [Online]. Available: www.eia.gov/forecasts/aeo/pdf/0383(2012).pdf?

[21] A. Debs, *Modern power systems control and operation*. Kluwer Academic Publishers, Norwell, MA, 1988.

[22] V. Vittal and A. Bergen, *Power systems analysis*. Prentice Hall, 1999.

[23] P. Kundur, N. Balu, and M. Lauby, *Power system stability and control*. McGraw-hill New York, 1994, vol. 4, no. 2.

[24] J. Lofberg, "Yalmip: A toolbox for modeling and optimization in matlab," in *Int. Symp. Computer Aided Control Systems Design*, 2004, pp. 284–289.

[25] (2012, Feb.) IBM ILOG CPLEX Optimizer. [Online]. Available: www.ibm.com/software/integration/optimization/cplex-optimizer/